Tunnel Transit-Time (TUNNETT) Devices for Terahertz Sources*

G. I. Haddad and J. R. East
Solid-State Electronics Laboratory
Department of Electrical Engineering and Computer Science
University of Michigan
Ann Arbor, Michigan, 48109-2122

Abstract

The potential and capabilities of Tunnel Transit-Time (TUNNETT) Devices for power generation in the 100–1000 GHz range are presented. The basic properties of these devices and the important material parameters which determine their properties are discussed and criteria for designing such devices are presented. It is shown from a first order model, that significant amounts of power can be obtained in this frequency range.

*This work was supported by the Center for Space Terahertz Technology under Contract No. NAGW-1334 and U. S. Army Research Office under the URI Program, Contract No. DAAL03-87-K-0007.

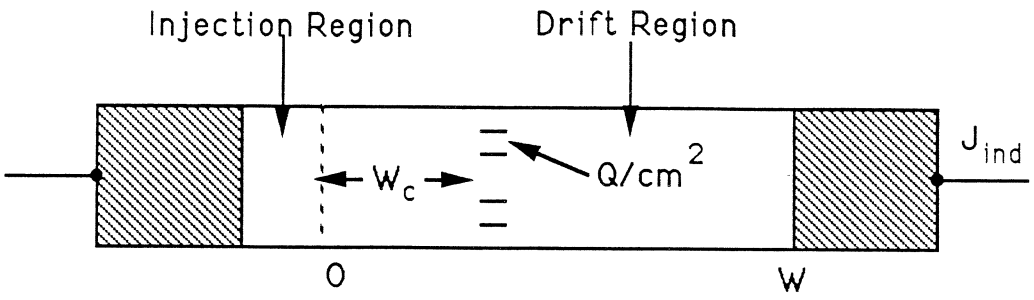

Figure 1 Two-Terminal Negative Resistance Transit-Time Device

1. Introduction

Two-terminal transit-time devices such as IMPATTS are capable of generating significant amounts of power at high-frequencies [1–3]. However, because of the avalanche process, they are very noisy and their efficiency decreases significantly at extremely high frequencies. Also, because of the very narrow drift regions and high doping densities required at such high frequencies, tunneling mechanisms become dominant and effect the performance. Through proper design of the device, we can take advantage of the very fast tunneling process to obtain extremely high frequency and reduce the noise. Such devices have been considered previously [4–7] and preliminary experimental results have been obtained in the 100–300 GHz range. Recent advances in material growth and processing technology will make a significant impact on further development of such devices.

In this paper, the basic principles of two-terminal transit-time devices will be presented and the differences among the various charge injection mechanisms will be discussed. This is followed by an assessment of the R.F. power generation capability of TUNNETTS as well as device design for various operating frequencies.

2. Basic Principles of Two-Terminal Negative Resistance Transit Time Devices

Two-terminal transit time negative resistance devices generally consist of a charge injection region and a drift region as shown in fig. 1. There are several means of injecting the charge Q into the drift region. These include:

a) Thermionic Emission Over a Barrier (BARRITT):
This can be realized from a forward-biased p^+- n or n^+- p junction or by incorporating a wide band semiconductor layer to form a heterojunction barrier.

b) Tunneling Through a Barrier (TUNNETT):
This can be realized by tunneling through a single heterojunction barrier, resonant tunneling through a double barrier [8,9] or tunneling in a reverse-based p^+- n^+ junction.

c) Avalanche Multiplication (IMPATT):
This is realized through avalanche breakdown.

d) Mixed Tunneling or Thermionic Emission and Avalanche Multiplication (MITATT):
This results when two types of mechanisms are involved in the charge generation.

When a pulse of charge of Q coulombs/cm^2 is injected into the drift region and travels with a velocity v_Q in the drift region, the current density induced in the external circuit is given by

$$J_{ind} = \frac{Q}{W}\left[v_Q - \frac{W_c}{W}\frac{dW}{dt}\right] \tag{1}$$

where

W = the width of the depletion layer
and W_c = the location of the charge Q.

For the sake of simplicity and since most of the devices of interest here will be punched through at the bias voltage, and the device is designed to maintain a high field in the drift region, we can assume that W is constant and $v_Q = v_s$, where v_s is the saturated velocity.

Under these conditions, the current voltage waveforms (under large signal conditions which are of interest here) for all of the above devices can be represented approximately as shown in fig. 2. In this figure,

V_{dc} = the d.c. voltage (V)

V_{RF} = the magnitude of the R.F. voltage (V)

Θ_m = the phase angle of charge injection (rad.)

Θ_w = the phase width of the injected charge pulse (rad.)

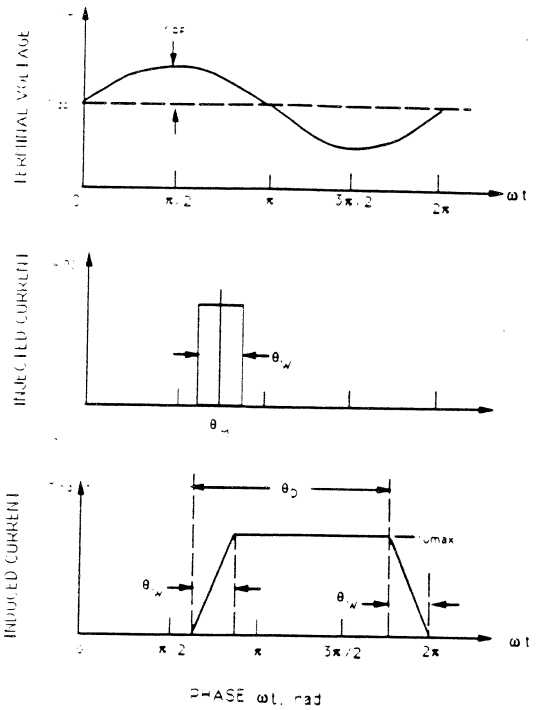

Figure 2 Idealized Voltage and Current Waveforms for Two-Terminal Transit-Time Devices

Θ_D = the drift region transit angle (rad)
$= \omega\tau_D = \omega W/v_s$

τ_D = the transit time through the drift region (sec.)

J = the current density (A/cm^2)

From the waveforms shown in fig. 2, it can be easily shown that the RF power density (watts/cm^2) can be expressed as,

$$P_{RF} = \frac{1}{2\pi}\int_0^{2\pi} J_{ind}(\omega t) V_{RF}\ \sin(\omega t)\ d(\omega t) \tag{2}$$

which simplifies to

$$P_{RF} = V_{RF} J_{dc} \left(\frac{\sin(\Theta_w/2)}{\Theta_w/2}\right)\left(\frac{\cos\Theta_M - \cos(\Theta_M + \Theta_D)}{\Theta_D}\right) \tag{3}$$

The device efficiency is

$$\eta \triangleq \frac{P_{RF}}{P_{dc}} = \left(\frac{V_{RF}}{V_{dc}}\right)\left(\frac{\sin(\Theta_w/2)}{\Theta_w/2}\right)\left(\frac{\cos\Theta_M - \cos(\Theta_M + \Theta_D)}{\Theta_D}\right) \tag{4}$$

Θ_M and Θ_w result primarily from the device design of the generation region and this will determine the particular mode of operation.

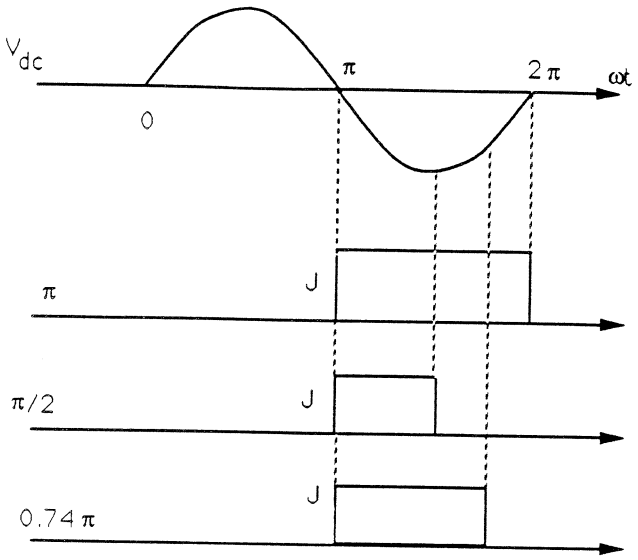

Figure 3 Current Voltage Waveforms for the IMPATT MODE

For IMPATT mode operation, $\Theta_M \cong \pi$ and η becomes

$$\eta = \left(\frac{V_{RF}}{V_{dc}}\right)\left(\frac{\sin(\Theta_w/2)}{\Theta_w/2}\right)\left(\frac{\cos\Theta_D - 1}{\Theta_D}\right) \quad . \tag{5}$$

For maximum η (negative for power delivery), we would like Θ_w to be as small as possible. This implies a small charge-generation region width, small voltage drop across the generation region and V_G/V_D as small as possible, where V_G is the voltage across the generation region and V_D is the voltage across the drift region.

As an ideal case, let $\Theta_w \rightarrow 0$ (very sharp pulse). This assumption is made for simplicity since we are interested here in a first order estimation. Even if Θ_w is $\pi/2$ (which is quite wide for most cases), the estimates will be reduced by a factor of $2/\pi$ which is small relative to the estimates of interest here.

For this case we have

a. $\Theta_m \cong \pi$ (IMPATT mode)

$$\eta = \frac{V_{RF}}{V_{dc}}\left(\frac{\cos\Theta_D - 1}{\Theta_D}\right) \quad . \tag{6}$$

For $\Theta_D = \pi$, $\eta = -(2/\pi)(V_{RF}/V_{dc})$, for $\Theta_D = \pi/2$, $\eta = -(2/\pi)(V_{RF}/V_{dc})$, and for $\Theta_D = 0.74\pi$, η = - $(2.27/\pi)$ (V_{RF}/V_{dc}). The current voltage waveforms for these cases are illustrated in fig. 3.

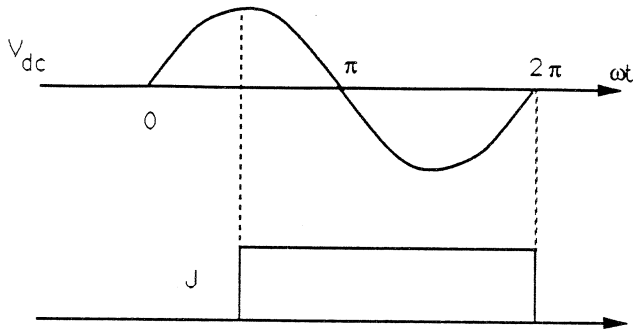

Figure 4 Current-Voltage Waveforms for TUNNETT and BARRITT Devices

It is worth noting that the d.c. voltage is directly proportional to the width of the drift region and thus to Θ_D. Since the R.F. voltage is directly proportional to the d.c. voltage, then the R.F. power density will be directly proportional to Θ_D. Also the capacitance of the device is inversely proportional to Θ_D (or W) and thus it is desirable (as will be shown later) from an impedance matching consideration to make Θ_D or W as large as possible for maximizing power. Thus even though the efficiency for $\Theta_D = \pi/2$ or π is the same, the power generation capability will be much higher for the $\Theta_D = \pi$ case.

It is also important to point out that in an actual device, Θ_m will be less than π and thus a minimum drift angle is required before the device exhibits a negative resistance. Therefore a frequency will exist, usually referred to as the avalanche frequency ωa, below which the resistance will be positive. This is desirable since it will then be easier in such a device to eliminate bias-circuit oscillations which would be difficult to suppress if the negative resistance extended all the way to d.c. Such a device will then exhibit a negative resistance (and thus is capable of oscillation) between ωa and $\omega\tau_D = 2\pi$. It will also have islands of negative resistance at higher frequencies but with much reduced power generation capability.

b. For $\Theta_m = \pi/2$ (TUNNETT, BARRITT)

$$\eta = (V_{RF}/V_{dc})(\sin\Theta_D/\Theta_D) \quad . \tag{7}$$

For $\Theta_D = (3\pi/2)$, $\eta = -(2/3\pi)(V_{RF}/V_{dc})$. The current voltage waveforms for this case are shown in fig. 4. It is seen that, compared to an IMPATT device, the efficiency is approximately 1/3 for this case. However, the voltage will be approximately 3/2 because $\Theta_D = 3\pi/2$ instead of π and the capacitance will be lower which is also

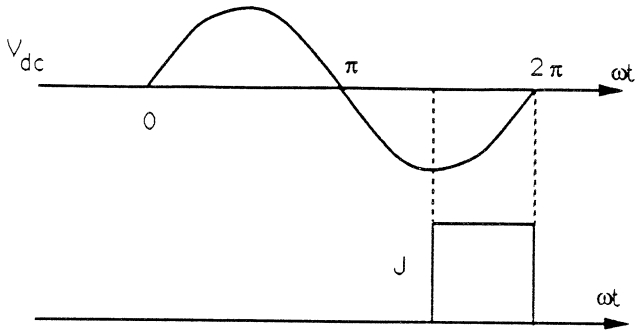

Figure 5 Current-Voltage Waveform for a QWITT Device

desirable. It is also seen that the device will exhibit a negative resistance between $\omega\tau_D = \pi$ and 2π and thus will not exhibit a negative resistance at low frequencies which is an important consideration for bias-circuit oscillations.

c. For $\Theta_m = 3\pi/2$ (Resonant-Tunneling Injection: QWITT)

$$\eta = (V_{RF}/V_{dc})\frac{\sin\Theta_D}{\Theta_D} \quad . \tag{8}$$

For $\Theta_D = \pi/2$, $\eta = -\frac{2}{\pi}\frac{V_{RF}}{V_{dc}}$. The current-voltage waveform for this case is shown in fig. 5.

It is worth noting for this case that if this particular mode of injection is employed, the negative resistance will exist all the way to d.c. This makes it difficult to stabilize such devices and spurious oscillations and in particular bias circuit oscillations will be extremely difficult to suppress. In addition the magnitude of the R.F. voltage swing for this case will be extremely small and thus the power generation capability will be very limited. Also depending on the bias point, if the R.F. voltage magnitude is increased, injection at $\Theta_m = \pi/2$ will take place which will be out of phase with the $\Theta_m = 3\pi/2$ case and will decrease the negative resistance and thus the power output significantly. Therefore, operation of such a device in the transit-time mode is not desirable and is probably best to minimize transit-time effects and utilize the inherent negative resistance property. However, the problems of small power output and spurious oscillations will persist.

d. Ideal case for η.

The maximum η is obtained for $\Theta_w = 0$, $\Theta_m = 3\pi/2$ and $\Theta_D \approx 0$. For this case, $\eta = -(V_{RF}/V_{dc})$. The current voltage waveform for this case is shown in fig. 6. However, the R.F. power generated will be small because Θ_D and thus V_{dc} will be very

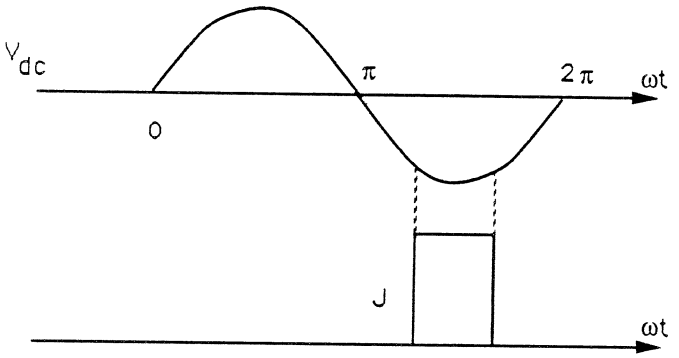

Figure 6 Current-Voltage Waveform for Ideal Efficiency

small. This does point the way, however, to shape the current-voltage characteristic to optimize η if that becomes an important factor.

Since we will be mostly concerned here with TUNNETT devices, fig. 7 shows a heterojunction structure for optimizing the efficiency by inserting spacer layers of GaAlAs. Since v_s in GaAlAs is approximately 1/5 of the saturated velocity in GaAs, the current voltage waveform will be approximately as shown in fig. 7(b), where the induced current during the transit of electrons in the GaAlAs portion of the drift region will be directly proportional to the saturated velocity in this material. This would result in enhanced efficiency [5,7] as shown in fig. 8. It is seen, for example, that for $\beta = 0.2(v_{s_{GaAlAs}} = 0.2v_{s_{GaAs}})$, the efficiency of a heterojunction-type device can approach that of a conventional IMPATT. Thus, heterojunctions can be employed effectively and in several different configurations to enhance the efficiency and power output of TUNNETT devices. This is an extremely important aspect of recent advances in material growth technology which will aid in improved performance of such devices.

3. TUNNETT Device Design

The basic structure and electric-field profile at the bias point for a basic device are shown in fig. 9. The i-layer between the p^{++} and n^{+} regions is not necessary and can be eliminated. The drift region doping can be designed to optimize performance. This basic structure can operate in several modes depending on the i-layer thickness, x_A. It has been shown [5] that for a GaAs structure (which will be considered here), if $x_a > 1,000$ Å, $E_c x_A = 1$ and avalanche breakdown occurs and this results in an

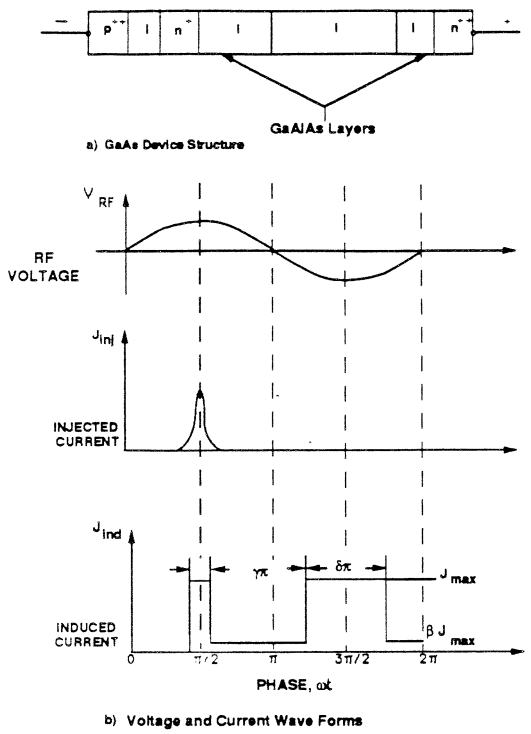

Figure 7 Heterojunction TUNNETT Device

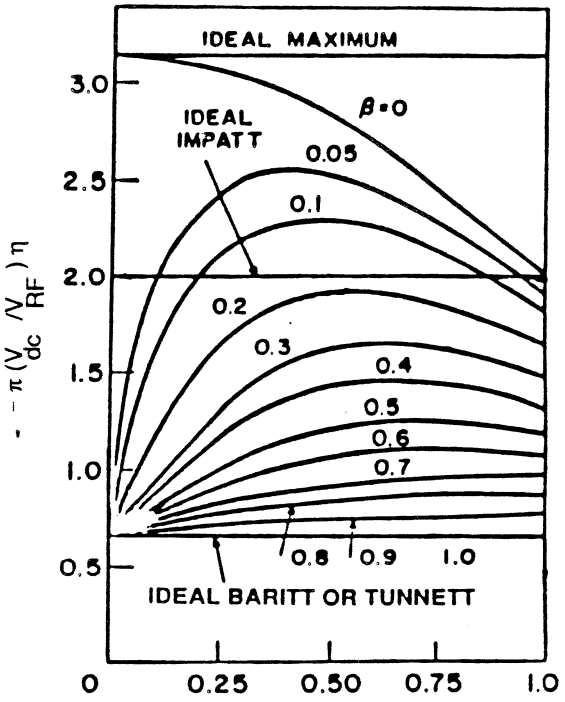

Figure 8 Efficiency as a Function of δ and β. ($\gamma = 0$)

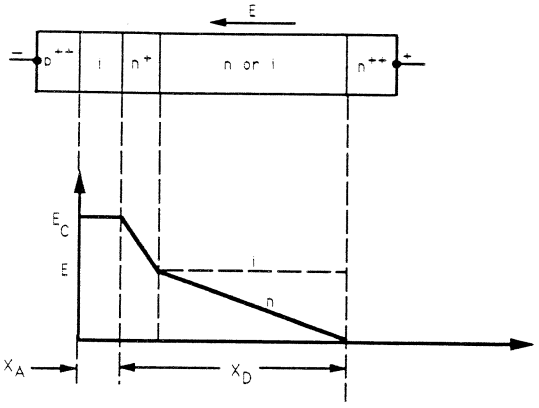

Figure 9 TUNNET Device

IMPATT device. If $x_A < 500$ Å, $E_c > 10^6$ V/cm, injection of carriers will be through tunneling and this results in a TUNNETT device. If 500 Å $< x_A <$ 1,000 Å, both tunneling and avalanche will be present and this results in a MITTAT device.

It is worth noting here that several means for improving the performance of such two-terminal negative resistance devices exist and such devices have the capability of generating significant amounts of power in the 100–1,000 GHz range. Such basic structures also result in very highly nonlinear capacitance-voltage characteristics before breakdown or tunneling occurs and thus will make excellent varactors for harmonic multiplication particularly when low power levels are available at the fundamental. Such devices do not exhibit an inherent negative resistance at low frequencies (except for rectification effects) and thus would be much easier to stabilize and suppress bias circuit oscillations.

4. Estimation of Expected Power Output From Conventional Single Drift TUNNETT Devices

Since we are interested in a first order estimate of the power generation capability, we will consider here a basic TUNNETT structure. As indicated earlier more complicated structures including hereojunctions and double-drift can be employed to improve performance. From the previous current-voltage waveform (fig. 4) for a TUNNET device ($\Theta_w = 0$, $\Theta_m = \pi/2$ and $\Theta_D = 3\pi/2$), the admittance per unit area can be expressed as,

$$Y_D = -G_D + jB_D$$

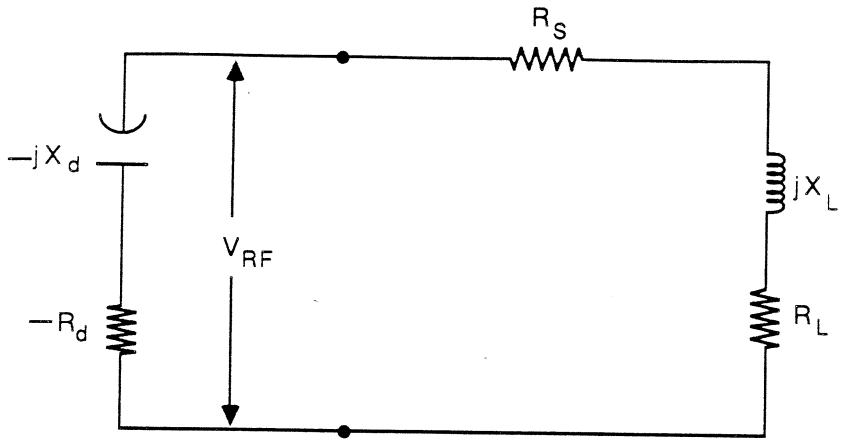

Figure 10 Oscillator Equivalent Circuit

$$= -\frac{4J_{dc}}{3\pi V_{RF}} + j\left[\frac{\omega\epsilon}{x_D + x_A} - \frac{4J_{dc}}{3\pi V_{RF}}\right] \tag{9}$$

$$Y_d = \text{the total admittance}$$

$$= AY_D = A[-G_D + jB_D] \tag{10}$$

where A = the area of the device (cm^2)

$$Z_d = \text{the total impedance of the device} = -R_d - jX_d$$

$$= \frac{1}{Y_D} = \frac{1}{A}\left[\frac{-G_D}{G_D^2 + B_D^2} - j\frac{B_D}{G_D^2 + B_D^2}\right] \tag{11}$$

The equivalent circuit for an oscillator is shown in fig. 10

where R_s = the parasitic diode resistance and circuit loss
R_L = the useful load resistance
and X_L = the load reactance.

From the oscillation conditions, we have

$$X_L = X_d \; ; \; R_d = R_s + R_L$$

$$\therefore \quad \frac{1}{A}\left[\frac{G_D}{G_D^2 + B_D^2}\right] = R_s + R_L$$

and

$$A = \left(\frac{G_D}{G_D^2 + B_D^2}\right) \frac{1}{R_s + R_L} \tag{12}$$

$$\begin{aligned} P_{RF}(Gen.) &= \frac{V_{RF}^2}{2} G_d = \frac{V_{RF}^2}{2}(AG_D) \\ &= \frac{V_{RF}^2}{2}\left(\frac{G_D^2}{G_D^2 + B_D^2}\right) \frac{1}{R_s + R_L} \end{aligned} \tag{13}$$

$$\begin{aligned} P_{RF}(R_L) &= \text{the power delivered to the load} \\ &= P_{RF}(Gen.) \frac{R_L}{R_s + R_L} \\ &= \frac{V_{RF}^2}{2}\left(\frac{G_D^2}{G_D^2 + B_D^2}\right) \frac{1}{R_L(1 + R_s/R_L)^2} \end{aligned} \tag{14}$$

For finite R_s, the maximum power delivered to R_L occurs when $R_s = R_L$. For this case we have,

$$P_{RF}(R_L)_{max} = \frac{V_{RF}^2}{2}\left(\frac{G_D^2}{G_D^2 + B_D^2}\right) \frac{1}{4R_L} \tag{15}$$

and

$$A = \left(\frac{G_D}{G_D^2 + B_D^2}\right) \frac{1}{2R_L} \tag{16}$$

Next we need to estimate V_{RF} and J_{dc}. For this we assume the following approximate electric-field profile at the d.c. bias point (as shown in fig. 11).

where x_A = the effective generation region width
x_D = the drift-region width
E_m = the maximum electric field in the tunneling region
E_D = the field in the drift region

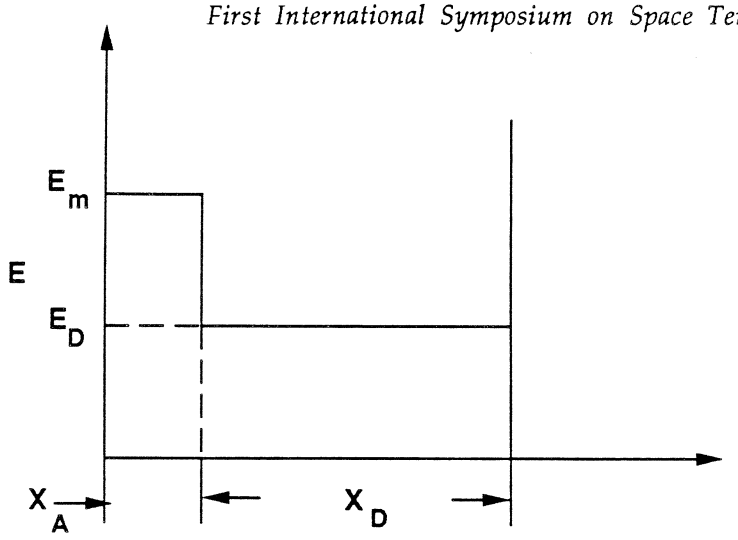

Figure 11 Approximate Electric Field Profile at the d.c. Bias Voltage

and

$$V_{dc} = (E_m - E_D)x_A + E_D(x_A + x_D) \quad . \tag{17}$$

If we assume that at V_{min} (the minimum dynamic voltage at $\omega t = \frac{3\pi}{2}$) $E = E_s$ where $v \geq v_{sat}$ for $E \geq E_s$, we find that,

$$V_{RF} = V_{dc} - V_{min} = E_D(x_A + x_D) - E_s(x_D + x_A) \tag{18}$$

and

$$\frac{V_{RF}}{V_{dc}} = \frac{E_D - E_s}{E_D + (E_m - E_D)\frac{x_A}{x_A + x_D}} \quad . \tag{19}$$

For the magnitude of current densities which will be encountered $E_M \cong 1.6 \times 10^6 \mathrm{V/cm}$. With present technology $x_A = 100$ Å can be easily achieved. For TUNNETT devices $\omega\tau_D = \frac{3\pi}{2}$ and thus

$$x_D = \frac{3v_s}{4f} \quad . \tag{20}$$

It is important to keep carrier generation in the drift region very low. We will therefore assume that

$$\int_0^{x_D} \alpha \, dx = 0.1 \tag{21}$$

where α = ionization rate = $Ae^{-(b/E)^m}$.

For GaAs: $A = 3.85 \times 10^5/cm.$, $b = 6.85 \times 10^5 V/cm$ and $m = 2$

$$\therefore \quad Ae^{-(b/E_D)^2} \, x_D = 0.1 \tag{22}$$

and

$$E_D = \frac{b}{\left[ln\left(\frac{Ax_D}{0.1}\right)\right]^{1/2}} \quad . \tag{23}$$

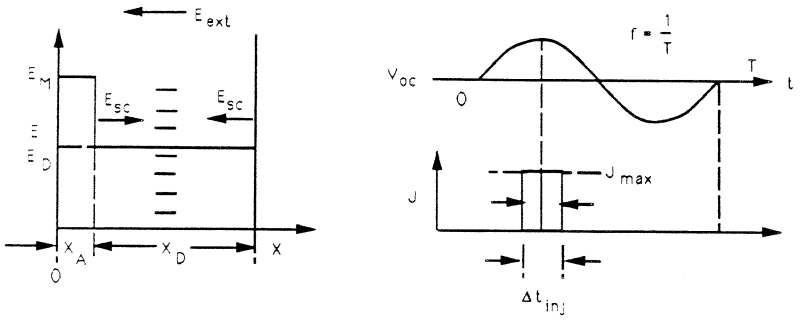

Figure 12 Electric Field and Injected Current Pulse for Estimating J_{dc}

Assuming $E_s = 3 \times 10^3$ V/cm. and an effective velocity $v_s = 10^7$ cm/sec. we then have the parameters shown in Table I for devices operating at different frequencies.

Next we estimate J_{dc} by considering space charge effects as shown in fig. 12. Assume $\Delta t_{inj} = R_{inj}T$ where R is a constant fraction $= \Theta w/2\pi$.

The total charge in the drift region $= AJ_{max}\Delta t_{inj}$

$$= qA \int_0^{x_D} n(x')\, dx' \tag{24}$$

$$\frac{dE_{sc}}{dx} = \rho/\epsilon = \frac{-qn(x)}{\epsilon}$$

$$\Delta E(x) = E(x) - E(o) = \frac{-q}{\epsilon} \int_0^x n(x')dx' \tag{25}$$

$$\Delta E = \Delta E(x_D) = E(x_D) - E(o) = \frac{-q}{\epsilon} \int_0^{x_D} n(x')dx' = \frac{-q}{\epsilon} \left[\frac{J_{max}\Delta t_{inj}}{q}\right] \tag{26}$$

$$|\Delta E| = \frac{J_{max}R_{inj}T}{\epsilon} \leq E_D \tag{27}$$

$$J_{DC} = \frac{J_{max}\Delta t_{inj}}{T} = J_{max}R_{inj}$$

$$\therefore J_{DC} \leq \epsilon\, E_D\, f \quad . \tag{28}$$

From an estimate of V_{dc}, V_{RF} and J_{dc}, the equations given above can be employed in a straightforward manner to estimate the R.F. power which can be expected from such devices.

We will first assume that $R_s + R_L = 1\Omega$, which is unrealistic but serves as a good reference for other more realistic cases. The pertinent parameters for this case are shown in Table II.

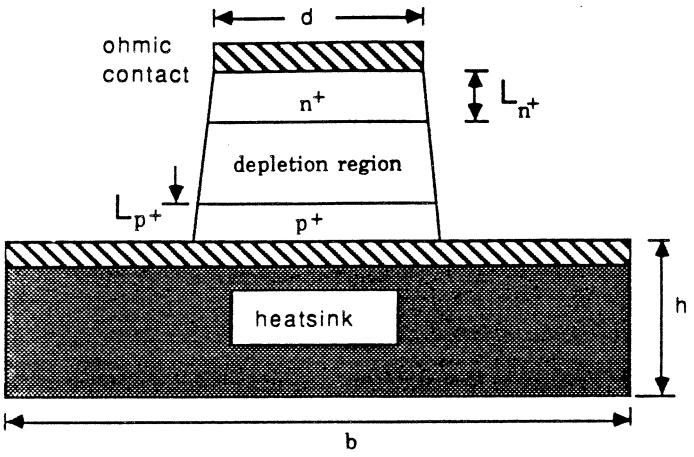

Figure 13 Mesa Diode Structure

The series resistance represents power loss and is extremely important for these devices. Figure 13 is a cross-sectional view of a mesa diode. The total positive resistance, R_s, associated with the mesa diode is given by [10]

$$R_s(f) = \frac{\rho_c + \rho_e L_e}{A} + \frac{\rho_s}{\pi\sigma}\left[0.5 \ln (b/d) + h/b\right] \quad . \tag{29}$$

Where,

ρ_c is the specific contact resistance in $\Omega - cm^2$ (1×10^7)
ρ_e is epilayer resistivity in ohms-cm ($\rho_n = 0.00037$, $\rho_p = 0.0015$)
ρ_s is the resistivity of the heatsink (gold) in ohms-cm (0.00024)
L_e is the length of the undepleted epilayers ($L_{n+} = 0.5\mu$m, $L_{p+} = 0.1\mu$m)
A is the area of the diode
σ is the skin depth given by $\sqrt{\frac{2\rho_s}{\mu\,\omega}}$
b is the length of the chip (0.02 cm)
h is the height of the substrate or heatsink (0.005 cm)
d is the diode diameter.

The series resistance is given in Table III. Taking into account the series resistance, the amount of useful power delivered to R_L is reduced. The results for different diameter devices at the center frequencies of 100, 500 and 1,000 GHz are shown in Tables IV, V and VI respectively.

Another important parameter for cw operation is the thermal resistance which is approximately given by

$$R_{th} = \frac{2}{\pi K_{hs} d} + \frac{4L}{\pi d^2 K_{sc}} \tag{30}$$

where,

K_{hs} : Thermal conductivity of the heatsink in $W/\text{cm}\ ^\circ\text{K}$ (3.9 for Cu and 11.7 for diamond)

K_{sc} : Thermal conductivity of the semiconductor in $W/\text{cm}\ ^\circ\text{K}$ (0.3 for GaAs)

L_{p+} : The distance from the junction to the heatsink in cm (0.1 μm)

d : is the diode diameter in cm.

The thermal resistance is given in Table VII for different diameters and heat sinks.

From the thermal resistance values given in Table VII, we can estimate the temperature rise in the device for various operating conditions and device diameters. This is done in Table VIII. It can be seen from this table that the diameters chosen for the 100 and 500 GHz operation result in a temperature rise of less than 225°K which is a safe value. However, for 1,000 GHz a diamond heatsink is required to remain below the 225°K temperature rise. Therefore, for this case, $J_{d.c.}$ must be reduced for a copper heatsink. For example for a 4 μm-diameter device $\Delta T = 363$°K. In order to limit ΔT to 225°K and maintain the same load impedance, we can reduce $J_{d.c.}$ by a factor of 0.62. This will reduce the R.F. power by a factor of 0.38 and thus result in an output power of 2.8 mw which is still significant.

5. Conclusions

Preliminary estimates of the power generation capability of TUNNETT devices in the 100–1,000 GHZ range are promising. It is believed that an output power of 1 mw at one terahertz is feasible.

Acknowledgement: The authors are grateful to R. Mains and I. Mehdi for their contributions to this work.

REFERENCES

[1] R. K. Mains and G. I. Haddad, "Properties and Capabilites of Millimeter–Wave IMPATT Diodes," *Infrared and Millimeter-Waves*, K. J. Button (Ed.), vol. 10, Part III, Chap. 3, Academic Press, Inc., New York, 1963.

[2] R. K. Mains, G. I. Haddad, and P. A. Blakey, "Simulation of GaAs IMPATT Diodes Including Energy and Velocity Transport Equations," *IEEE Trans. on Electron Devices*, vol. Ed–30, No. 10, pp. 1327–1338, October 1983.

[3] M. El-Gabaly, G. I. Haddad, and R. K. Mains, "Effect of Doping Profile Variation on GaAs Hybrid and Double-Read IMPATT Diode Performance at 60 and 94 GHz," *IEEE Trans. on Microwave Theory and Techniques*, vol. MTT–32, No. 10, pp. 1342–1352, October 1984.

[4] J. Nishizawa, K. Mofoya, and Y. Okuno, "GaAs TUNNETT Diodes," *IEEE Trans. on Microwave Theory and Techniques*, vol. MTT–20, No. 12, pp. 1029–1035, December 1978.

[5] M. Elta and G. I. Haddad, "High-Frequency Limitations of IMPATT, MITATT, and TUNNETT Mode Devices," (Invited Paper) *IEEE Trans. on Microwave Theory and Techniques*, vol. MTT–27, No. 5, pp. 442–449, May 1979.

[6] M. E. Elta, H. R. Fetterman, W. V. Macropoulas, and J. J. Lambert, "150 GHz GaAs MITATT Source," *IEEE Electron Device Letters*, vol. EDL–1, No. 6, pp. 115–116, June 1980.

[7] N. S. Dogan, J. R. East, M. E. Elta, and G. I. Haddad, "Millimeter-Wave Heterojunction MITATT Diodes," *IEEE Trans. on Microwave Theory and Techniques*, vol. MTT–35, No. 12, pp. 1308–1317, December 1987.

[8] T.C.L.G. Sollner, E. R. Brown, W. D. Goodhue, and H. Q. Le, "Observation of millimeter-wave tunneling diodes and some theoretical considerations of ultimate frequency limits," *Appl. Phys. Lett.*, vol. 50, No. 6, pp. 332–334, February 1987.

[9] V. P. Kesan, D. P. Neikirk, B. G. Streetman, and P. A. Blakey, "A New Transit-Time Device Using Quantum-Well Injection," *IEEE Electron Device Letters*, vol. EDL-8, No. 4, pp. 129–131, April 1987.

[10] L. E. Dickens, "Spreading Resistance as a Function of Frequency," *IEEE Trans. on MTT*, vol. MTT-15, No. 2, pp. 101–109, February 1967.

TABLES

Table I. Important Device Parmeters for Different Center Frequencies

f(GHz)	$x_D(\mu m)$	$E_D(V/cm)$	$V_{dc}(V)$	$V_{RF}(V)$	V_{RF}/V_{dc}
100	0.75	2.1×10^5	17.4	15.7	0.90
500	0.15	4.13×10^5	7.8	6.5	0.84
1000	0.075	6.6×10^5	6.5	5.5	0.83

Table II. Estimated $P_{RF}(Gen.)$ and Other Operating Parameters for a 1-Ω Reference ($R_s + R_L = 1\Omega$)

f(GHz)	$V_{dc}(V)$	$V_{RF}(V)$	$J_{dc}(A/cm^2)$	$G_D\left(\frac{mho}{cm^2}\right)$	$B_D\left(\frac{mho}{cm^2}\right)$	A (cm^2)	$D(\mu m)$
100	17.4	15.7	22.3×10^3	0.6×10^3	8.2×10^3	8.87×10^{-6}	34
500	7.8	6.5	2.2×10^5	1.4×10^4	1.9×10^5	3.9×10^{-7}	7
1000	6.6	5.5	7×10^5	5.4×10^4	7.3×10^5	1.0×10^{-7}	3.6

f	I_{dc}(ma)	P_{dc}(W)	η (%)	$P_{RF}(Gen.)$T(mW)
100	198	3.44	19	650
500	85.8	0.67	18	120
1000	70	0.46	17.5	80

Table III. Series Resistance of Mesa Diode

diameter	diode series resistance (Ω) at		
μm	100 GHz	500 GHz	1000 GHz
1	13.6	14.6	15.4
2	3.9	4.8	5.5
3	2.0	2.9	3.5
4	1.4	2.2	2.7
5	1.1	1.8	2.3
7	0.79	1.4	1.9
10	0.60	1.2	1.6
15	0.46	0.96	1.3
20	0.39	0.84	1.2
25	0.35	0.75	1.0
30	0.31	0.68	0.95

Table IV. Estimated Power Output Including R_s
$f = 100$ GHZ
$J_{dc} = 22.3 \times 10^3 A/cm^2$; $V_{dc} = 17.4V$; $V_{RF} = 15.7V$

Diode Diam. (μm)	Area (cm^{-2})	$R_s(\Omega)$	$-R_d(\Omega)$	$R_L(\Omega)$	$I_{dc}(ma)$	P_{dc}(w)	P_{RF} (Gen.) (mw)	P_{RL} (R_L) (mw)	$\eta\%$
20	2.9×10^{-6}	0.39	3	2.61	66	1.15	217	189	16.4
25	4.5×10^{-6}	0.35	2.4	2	100	1.75	271	225	13
30	6.5×10^{-6}	0.31	2	1.69	145	2.52	325	275	11
30	6.5×10^{-6}	1	2	1	145	2.52	325	162	6.4

Table V. Estimated Power Output Including R_s
$f = 500$ GHz
$J_{dc} = 2.2 \times 10^5 A/cm^2$; $V_{dc} = 7.8V$; $V_{RF} = 6.5V$

Diode Diam. (μm)	Area (cm^{-2})	$R_s(\Omega)$	$-R_d(\Omega)$	$R_L(\Omega)$	I_{dc}(ma)	P_{dc}(mw)	P_{RF} (Gen.) (mw)	P_{RL} (R_L) (mw)	$\eta\%$
4	1.16×10^{-7}	2.2	3.36	1.16	25.5	200	35	12	6
5	1.8×10^{-7}	1.8	2.16	0.36	39.6	309	55	9.2	3
7	3.9×10^{-7}	1.4	1	–	–	–	–	–	–

will operate at a lower V_{RF}

Diode Diam. (μm)	Area (cm^{-2})	$R_s(\Omega)$	$R_L(\Omega)$	$-R_d(\Omega)$	$V_{RF}(V)$	I_{dc}(ma)	P_{dc}(mw)	P_{RF} (Gen.) (mw)	P_{RL} (R_L) (mw)	$\eta\%$
4	1.16×10^{-7}	2.2	2.2	4.4	4.96	25.5	200	27	13.5	6.75
5	1.8×10^{-7}	1.8	1.8	3.6	3.9	39.6	309	33	16.5	5.3
7	3.9×10^{-7}	1.4	1.4	2.8	2.32	86	670	42.3	21	3
10	7.2×10^{-7}	1.2	1.2	2.4	1.46	158.4	1,235	49	24.5	2

Table VI. Estimated Power Output Including R_s
$f = 1000$ GHz
$J_{dc} = 7 \times 10^5 A/cm^2$; $V_{dc} = 6.6V$

(Because of series resistance, the device cannot oscillate at $V_{RF} = 5.5V$s where maximum η is obtained, but will oscillate at a lower V_{RF})

Diode Diam. (μm)	Area (cm^{-2})	$R_s(\Omega)$	$R_L(\Omega)$	$-R_d(\Omega)$	$V_{RF}(V)$	I_{dc}(ma)	P_{dc}(w)	P_{RF} (Gen.) (mw)	P_{RL} (R_L) (mw)	$\eta\%$
4	1.16×10^{-7}	2.7	2.7	5.4	0.88	81	535	15	7 .5	1.4
5	1.8×10^{-7}	2.3	2.3	4.6	0.66	126	832	17.6	8.8	1
7	3.9×10^{-7}	1.9	1.9	3.8	3.7	273	1,800	21	10.5	.5

Table VII. Thermal Resistance of a Mesa Diode

Diameter	R_{th} = Diode Thermal Resistance (10^2 °K/W)	
μm	Copper heatsink	Diamond heatsink
1	58.7	47.9
2	18.8	13.3
3	10.2	6.53
4	6.73	4.01
5	4.96	2.79
7	3.20	1.64
10	2.06	0.97
15	1.28	.055
20	0.92	0.38
25	0.72	0.29
30	0.59	0.23

Table VIII. Estimated CW Power

f(GHz)	Diode Diam. (μm)	$P_{dc}(w)$	$R_{th}(°/w)$ Cu	$R_{th}(°/w)$ Diamond	$\Delta T(°K)$ Cu	$\Delta T(°K)$ Diamond	$P_{RF}(mw)$
100	20	1.15	92	38	106	48	189
	25	1.75	72	29	126	51	225
	30	2.52	59	23	150	58	275
500	5	0.31	496	278	154	86	16.5
	7	0.67	320	164	214	110	21
	10	1.24	205	97	254	120	24.5
1000	4	0.54	673	401	363	216	7.5
	5	0.83	496	278	411	230	8.8
	7	1.8	320	164	576	295	10.5